GA–A25577

COMPATIBILITY OF THE RADIATING DIVERTOR WITH HIGH PERFORMANCE PLASMAS IN DIII-D

by
T.W. PETRIE, M.R. WADE, N.H. BROOKS, M.E. FENSTERMACHER,
M. GROTH, A.W. HYATT, R.C. ISLER, C.J. LASNIER, A.W. LEONARD,
M.A. MAHDAVI, G.D. PORTER, M.J. SCHAFFER, J.G. WATKINS,
W.P. WEST, and the DIII-D TEAM

OCTOBER 2006

GENERAL ATOMICS

DISCLAIMER

GA–A25577

COMPATIBILITY OF THE RADIATING DIVERTOR WITH HIGH PERFORMANCE PLASMAS IN DIII-D

by
T.W. PETRIE, M.R. WADE, N.H. BROOKS, M.E. FENSTERMACHER,*
M. GROTH,* A.W. HYATT, R.C. ISLER,† C.J. LASNIER,* A.W. LEONARD,
M.A. MAHDAVI, G.D. PORTER,† M.J. SCHAFFER, J.G. WATKINS,‡
W.P. WEST, and the DIII-D TEAM

This is a preprint of a paper to be presented at the 21st IAEA Fusion Energy Conference, October 16-21, 2006, in Chengdu, China, and to be published in the Proceedings.

*Lawrence Livermore National Laboratory, Livermore, California
†Oak Ridge National Laboratory, Oak Ridge, Tennessee
‡Sandia National Laboratories, Albuquerque, New Mexico

Work supported by
the U.S. Department of Energy
under DE-FC02-04ER54698, W-7405-ENG-48,
DE-AC05-00OR22725, and DE-AC04-94AL85000

GENERAL ATOMICS PROJECT 30200
OCTOBER 2006

GENERAL ATOMICS

Abstract

The radiating divertor concept was applied to high performance "hybrid" plasmas in both double-null (DN) and single-null (SN) configurations. The technique included: (1) injecting argon into the private flux region of the upper divertor, (2) enhancing the plasma flow into the inner and outer divertor targets by combining deuterium gas puffing upstream of the divertor targets with particle exhaust at the targets, and (3) isolating the upper inner and outer divertor legs with a structure in the private flux region. For high triangularity SN shapes, good confinement was maintained in the hybrid regime, while the peak heat flux at the *outer* divertor target was reduced by a factor of 2.5 and that at the *inner* target by 20%. The higher heat flux reduction at the outer target was caused by a higher concentration of argon in the outer leg. Argon accumulation in the main plasma was modest ($n_{Ar}/ne \le 0.004$ on axis), although the argon profile was more peaked than the electron profile. For the high triangularity DN shape, where particles were exhausted from *both* upper and lower divertors, the accumulation of argon in the core plasma of DNs was significantly higher than that of SNs under similar operating conditions. Prior to argon injection, the amount of the radiated power coming from the upper divertor was comparable to that from the lower divertor. With argon injected at a perturbing level, however, a 50% increase in radiation was observed from the upper divertor, but only a modest 5-10% increase from the lower divertor. Plasma detachment was not observed at either outer divertor target during steady state DN plasma operation at a perturbing argon injection level, where $\bar{n}_e/n_G \approx 0.7$ and $P_{RAD}/P_{IN} \approx 0.52$.

1. Introduction

Excessive thermal power loading on the divertor structures presents a problem for future, high-powered tokamaks such as ITER. This problem may be mitigated by "seeding" the divertor plasma with impurities that radiatively dissipate a significant fraction of the conducted power before it can reach the divertor targets. For this radiating divertor concept to be practical, leakage of the seeded impurity into the main plasma must not compromise the confinement and stability of the plasma. Leakage can be reduced by enhancing the flow of deuterium ions (D^+) into the divertor by combining upstream deuterium (D_2) gas puffing with particle exhaust at the divertor targets, i.e., "puff-and-pump" [1-2]. An enhanced particle flow toward the divertor targets exerts a frictional drag on impurities that inhibits their escape from the divertor. Such an approach may be particularly effective in a closed divertor, where baffling minimizes the direct paths of neutral impurity atoms back into the main chamber.

We report here on the application of the puff and pump scenario to hybrid H-mode plasmas [3] in both up/down-magnetically balanced and upwardly biased double-null (DN) shapes. The balanced DN shape is of particular interest, because higher values of τ_E and β_T are more readily achieved as the "triangularity" of the plasma shape is increased by pulling the X-points closer to the tokamak centerpost. Since higher overall triangularity (δ) can be achieved more readily in DN shapes than in single-null (SN) shapes, the DN is potentially more attractive as a basis for future generation high performance tokamaks. With the recent

modifications of the lower DIII-D divertor (described below), it now becomes feasible to study these high-δ DN plasmas under puff-and-pump conditions.

We focus here on the hybrid H-mode regime, because it is robust under highly perturbing conditions, such as heavy deuterium gas puffing, and it is being considered as a possible basis for ITER operation. The hybrid regime has similarities with the conventional H-mode regimes with edge localized modes (ELMs), such as high confinement, e.g., $H_{\mathrm{ITER89P}} \geq 2$, where H_{ITER89P} is the energy confinement normalized to the 1989 ITER L-mode scaling [4]. It mainly differs from the conventional H-mode regime, in that sawteeth are absent (or nearly absent). The absence of sawteeth is favorable to high performance plasma operation, since sawteeth can trigger the deleterious $m = 2,\ n = 1$ neoclassical tearing mode (NTM), which can limit the plasma confinement or even disrupt the plasma. (In its place, the mostly benign 3/2 NTM is typically present.)

The experimental arrangement and methodology are described in Section 2. In Section 3 we present results from our study of (1) SN and (2) DN puff-and-pump cases. A discussion of these results is presented in Section 4.

2. Experimental Setup

In studying hybrid plasmas under radiating divertor conditions, we take advantage of DIII-D's plasma shaping and particle removal capabilities in high-δ, SN and DN shapes. In 2005, our radiating divertor studies focused on a DN, cross-sectional shape that was *biased upward* ($dRsep = +1.0$ cm), as shown in Fig. 1(a). For purposes of discussion, we will refer to this shape as "single-null". In that study, in-vessel pumping of deuterium and argon (the seeded impurity) was done by cryo-pumps located inside the *upper outer* and *upper inner* diveror pumping plenums, indicated "plus" and "minus" in the respective plenums [5]. To increase the ion D^+ flow toward these two pumps, deuterium gas was introduced near the bottom of the vessel. Argon (Ar) was injected directly into the private flux region (PFR) of the upper divertor near the outer divertor target in all cases reported here. The divertor plasma occupies the shaded region above the dashed line in Fig. 1(a).

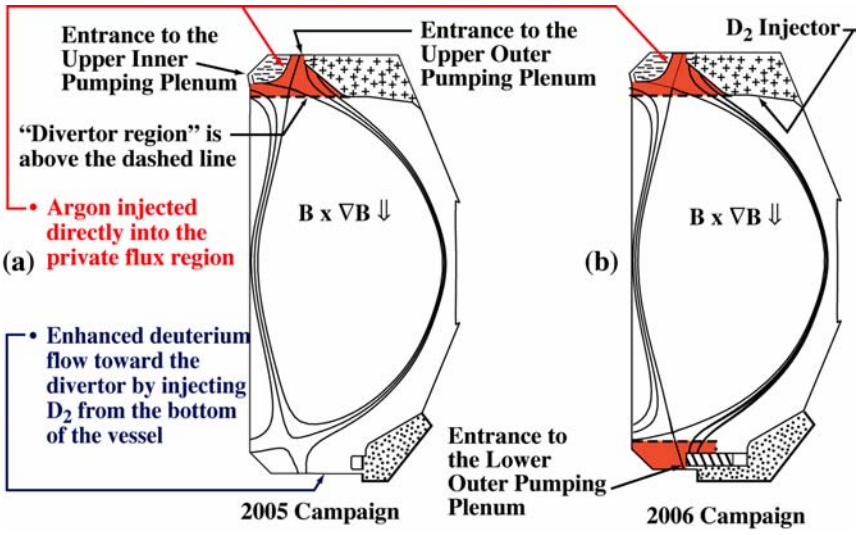

Fig. 1. Particle pumping and gas injection locations are superimposed on the single-null and double-null plasma cross-sections used in this study. The divertors are the orange shaded regions. (a) 2005 campaign and (b) 2006 campaign.

After the 2005 campaign, the lower divertor of DIII-D was modified to enable pumping of the lower outer leg of high-δ DN plasmas. The hatched region in Fig. 1(b) represents the extended shelf that was installed to direct neutrals from the recycling region near the lower outer strike point the to (lower divertor) pumping plenum, shown as "dots" in Fig. 1(b). This modification allows

particle pumping to be done simultaneously from both divertors, thus making it possible to study puff-and-pump scenarios in DN. Argon in the 2006 experiment was again injected directly into the PFR of the upper divertor. However, deuterium gas in 2006 was injected from a location just above the outer midplane, not from the bottom of the vessel (2005). The upper and lower divertor regions are illustrated by the shaded areas in Fig. 1(b).

Typical operating parameters for these experiments were: plasma current I_p = 1.2 MA, toroidal field B_T = 1.7 T with the $B \times \nabla B$ ion drift directed downward, $q_{95} = 4.3$, power input P_{IN} = (5.8–6.9) MW, line-averaged density $\bar{n}_e \approx (0.60 - 0.75) \times 10^{20}$ m^{-3} (or $\bar{n}_e / n_G \approx$ 0.55–0.70, where n_G is the Greenwald density [6]), and $H_{ITER89P} \approx 2$. All discharges had Type-1 ELMs [7]. Argon was selected as the seeded impurity because it radiates effectively at the temperatures prevailing in the divertor and pedestal regions of DIII-D hybrid H-mode plasmas and has a relatively short ionization mean free path. Carbon is the dominant intrinsic impurity in DIII-D discharges.

A useful figure of merit to characterize how effectively the injected Ar impurities are kept out of the main plasma is *exhaust enrichment* η_{exh}, i.e., $f_{Ar,exh} / f_{Ar,core}$. The quantity $f_{Ar,core}$ is the ratio of argon ion density to electron density in the main plasma and $f_{Ar,exh}$ is the ratio of the neutral Ar pressure in the outer pump plenum to the atomic-equivalent pressure of D_2 in this plenum. To determine $f_{Ar,core}$, absolute measurements of the spatial profiles of He-like argon densities in the main plasma were made using charge-exchange recombination spectroscopy [8]. The electron density (n_e) profiles were from Thomson scattering. To determine $f_{Ar,exh}$, simultaneous measurements of the Ar and D_2 partial pressures in the exhaust gas were made by a modified Penning gauge attached to the outer plenum [9].

The argon concentration $f_{Ar,core}$ was evaluated at radial location $\rho = 0.7$, located ≈ 10 cm inboard of the outer midplane separatrix. This location was chosen, because analysis with the multiple impurity species transport (MIST) code [10] indicated that helium-like argon (i.e., Ar^{+16}) was by far the dominant charge state of Ar at $\rho = 0.7$. Thus, the measured density of Ar^{+16} ($n_{Ar^{+16}}$) is a good approximation for the *total* Ar density (n_{Ar}) at $\rho = 0.7$.

3. Results

3.1. Single-Null Plasmas (2005)

Increasing the gas injection rate of deuterium (Γ_{D2}) strongly increased exhaust enrichment and reduced the accumulation of argon in the core plasma (Fig. 2). Argon was injected at a steady "trace" level into three identically prepared hybrid plasmas, differing only by the steady state D_2 injection rate. The argon density was measured at $\rho = 0.7$. This trend in exhaust enrichment and n_{Ar} ($\rho = 0.7$) is consistent with an earlier DIII-D study [1]. As in the case of Ref. 1, it was not feasible to match the rate of particle removal and particle injection well enough to hold the core density constant for the three D_2 puff rates, i.e., $n_e = (0.47 \times 10^{20} - 0.61 \times 10^{20})$ m^{-3} for Γ_{D2} = (12–108) Torr l/s. The increase in the deuterium gas puff rate was accompanied by an increase in the Type-1 ELM frequency ν_{ELM} from 40-80 Hz. Since this increase in ν_{ELM} also inhibited the influx of argon through the pedestal layer into the main plasma, it becomes difficult to distinguish between the relative contribution of the scrape-off layer (SOL) flow and Type-1 ELMs in screening argon from the main plasma.

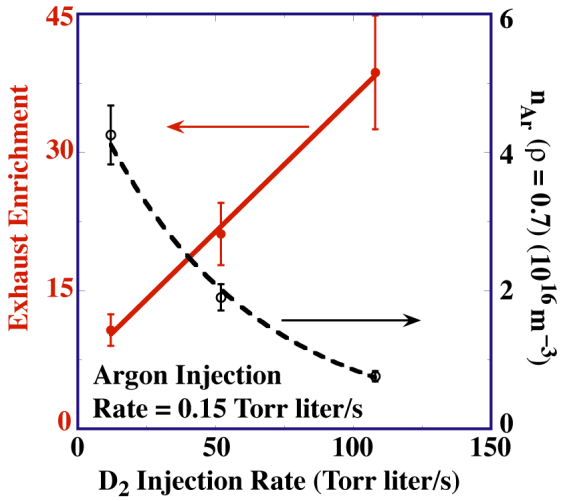

Fig. 2. η_{exh} and n_{Ar} at ($\rho = 0.7$) shown vs Γ_{D2}.

TABLE I: THREE LEVELS OF Γ_{Ar}

	Case 1	Case 2	Case 3
Γ_{D2} (Torr liter/s)	108	108	108
Γ_{Ar} (Torr liter/s)	0.15	1.95	3.8
n_e (10^{20} m^{-3})	0.61	0.64	0.67
H98Y2	2.0	2.0	2.0
P_{IN} (MW)	6.9	6.8	6.6
$P_{RAD,TOT}/P_{IN}$	0.45	0.52	0.63
$P_{RAD,MAIN}/P_{IN}$	0.17	0.21	0.24
$P_{RAD,DIV}/P_{IN}$	0.16	0.18	0.22
$q_{P,IN}$ (MW/m^2)	1.6	1.5	1.3
$q_{P,OUT}$ (MW/m^2)	3.0	1.8	1.2
$T_{e,IN}$ (eV)	10	10	10
$T_{e,OUT}$ (Ev)	22	15	10
ν_{ELM} (Hz)	$\approx$ 80	$\approx$ 75	$\approx$ 70
n_C/n_e ($\rho = 0.7$) (%)	2.1	2.1	2.2
n_{Ar}/n_e ($\rho = 0.7$) (%)	0.013	0.10	0.20
Z_{eff} ($\rho = 0.7$)	1.65	1.87	2.15
η_{exh}	38	37	33

Table I summarizes the response of hybrid H-mode plasmas to steady argon injection rates Γ_{Ar} at a trace level (Case 1) and at two different perturbing levels (Cases 2-3). The D_2 gas injection rate Γ_{D2} was fixed. Comparing Case 1 with Case 3 shows that the total radiated power fraction $P_{RAD,TOT}/P_{IN}$ increased from 0.45 to 0.63 between Case 1 and Case 3, with $\approx$ 45% of this increase in $P_{RAD,TOT}$ from the radiated power in the main plasma $P_{RAD,MAIN}$ and $\approx$ 40% from the divertor plasma $P_{RAD,DIV}$. The peak in the conducted heat flux to the outer divertor target $q_{P,OUT}$, as determined from Langmuir probe data, fell by a factor of $\approx$ 2.5, whereas the peak heat flux at the inner target $q_{P,IN}$ decreased only < 20%. The average electron temperature at the *outer* divertor target $T_{e,OUT}$ decreased from $\approx$ 22 to 10 eV, while that at the *inner* target remained steady at $T_{e,IN} \approx$ 10 eV in all three cases. Inner and outer divertor legs were attached during argon injection in each case. Finally, the Type 1 ELM frequency ν_{ELM} decreased from $\approx$ 80 to 70 Hz from Case 1 to Case 3.

Figure 3 shows that η_{exh} ($\rho = 0.7$) decreased weakly with increasing Γ_{Ar}, while $n_{Ar^{+16}}$ ($\rho = 0.7$) increased with Γ_{Ar} slightly faster than linear. The increase in Z_{eff} ($\rho = 0.7$) between Case 1 and Case 3 was almost entirely from the additional argon in the plasma. "Fuel dilution" due to Ar (i.e., $\approx 16 \times f_{Ar,core}$) was $\approx$ 0.032 at $\rho = 0.7$ in Case 3. In Table I the ratio $n_{C^{+6}}/n_e \approx$ 0.021 at $\rho = 0.7$ increased slightly with Γ_{Ar}.

The argon charge state distribution in steady state was evaluated with the MIST code for Case 3. MIST analysis is based on the measured n_e, T_e, and visible bremsstrahlung profiles, as well as spectrometer data of selected Ar lines [10]. Figure 4(a) indicates that $n_{Ar^{+16}}$ was 80%–85% of n_{Ar} at radius = 45 cm, which corresponds to $\rho \approx 0.7$. Near the plasma center, the Ar^{+17} and Ar^{+18} states became significant contributors to n_{Ar}. Ar^{+14} and Ar^{+15} gained in relative importance near the edge. The n_{Ar}-profile, based on MIST analysis, was clearly more peaked than the n_e-profile [Fig. 4(b)].

As Γ_{Ar} was raised, most of the increase in the bolometrically determined radiative emissivity ε_{RAD} occurred near the magnetic axis and near the plasma edge (Fig. 5). MIST analysis for

Case 3 shows that >80% of the *increase* in the measured $\varepsilon_{RAD}(\rho = 0)$ came from the line radiation of the Ar^{+16} and Ar^{+17} charge states, while several lower Ar charge states were strong contributors to the increase in ε_{RAD} near the edge. The Ar emissivity profile $\varepsilon_{RAD,Ar}$, as calculated by MIST, was peaked at the center and near the edge of the plasma with a deep trough between [Fig. 4(c)]. This is consistent with the changes in the measured ε_{RAD} profiles between Case 1 and Case 3 (Fig. 5). MIST analysis indicates that the increase in the radiated power from the main plasma between Case 1 and Case 3 resulted from the increase in Ar radiation. We estimate the Ar contribution to $P_{RAD,MAIN}$ was ≈ 30% in Case 3.

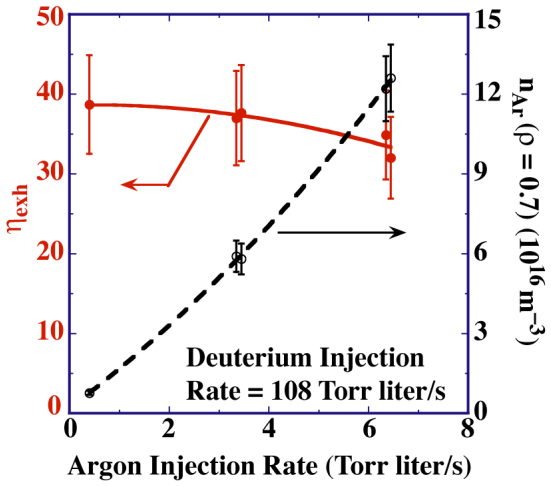

Fig. 3. η_{exh} and n_{Ar} at ($\rho = 0.7$) vs Γ_{Ar}.

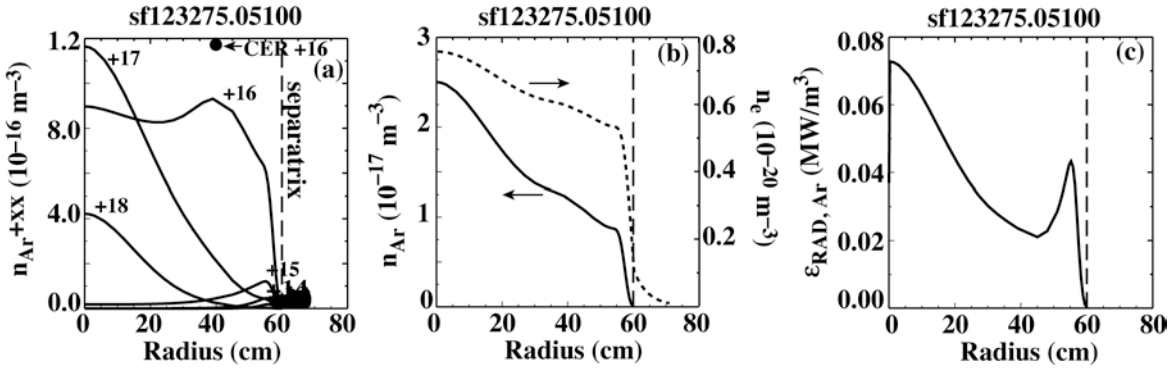

Fig. 4. MIST modeling of the "high" Γ_{Ar} shot (Case 3): (a) the density profile of the Ar charge states. (b) The n_{Ar}- and n_e-profiles. (c) The profile of the specific emissivity $\varepsilon_{RAD,Ar}$ due to argon.

Bolometric inversions indicate similarities and differences in the distribution of divertor radiated power between Case 1 and Case 3. Three areas of strong local emissivity in the divertor were observed: along the inboard divertor leg, along the outboard baffle, and near the outer divertor target. The Case 3 distribution had ≈ 2.5 times higher emissivity near the *outer* divertor target than Case 1. This local increase in the emissivity was coincident with the reduction in $q_{P,OUT}$. Little change in emissivity along the *inner* divertor separatrix was observed. The reduction in $q_{P,IN}$ was modest (i.e., 15%–20%) and could be ascribed largely to the decrease in the conductive/convective power flow out of the main plasma and the increased radiated power in the scrape-off layer plasma (SOL). Direct measurements of the

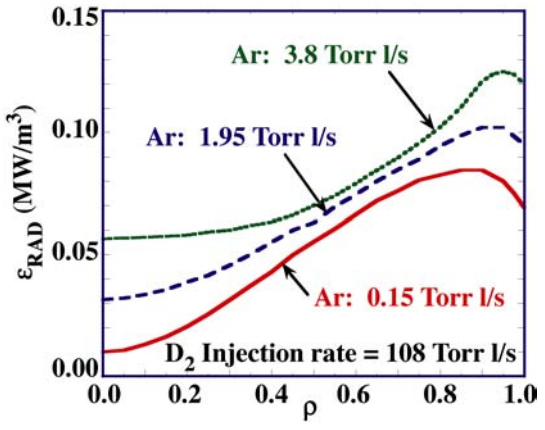

Fig. 5. The bolometrically measured radiated power densities ε_{RAD} for the three cases are plotted versus the normalized radial coordinate ρ.

separate contributions of argon, carbon, and deuterium to the divertor-radiated power were unavailable. Inferences from available spectroscopic and bolometric data indicate that $P_{RAD,DIV}$ was predominantly from carbon in Case 1. Carbon was still the primary radiator in Case 3, where we estimate an *upper* limit of 0.3 for the fraction of Ar radiation to $P_{RAD,DIV}$.

Measurements of Ar emission imply a higher concentration at the entrance to the outer divertor plenum than at the entrance to the inner. The ratio of Ar flux at the outer divertor target $\Phi_{Ar,OUT}$ to that at the inner target $\Phi_{Ar,IN}$ can be estimated by calculating their values from $\Phi = I \cdot S(T_e)/X(T_e)$, where I is the measured emission rate of the Ar II 434.8 nm line and S/X is the ratio of ionization and excitation rates computed from a collisional radiative model [11]. Because the electron temperature and density at *both* divertor targets were comparable in Case 3, i.e., ≈ 10 eV and $\approx 0.8\text{x}10^{20}$ m^{-3}, then $\Phi_{Ar,OUT}/\Phi_{Ar,IN}$ and $n_{Ar,OUT}/n_{Ar,IN}$ can be roughly estimated as $I_{ArII,OUT}/I_{ArII,IN}$, where $n_{Ar,IN}$ and $n_{Ar,OUT}$ are the Ar densities at the inner and outer targets, respectively. For Case 3, this ratio was ≈ 6, and the other two cases showed similar strong in/out asymmetry in Ar density.

3.2. Balanced DN Plasmas (2006)

More recently, we focused on the behavior of high triangularity, balanced *DN* plasmas under similar puff-and-pump conditions as discussed above for SNs, e.g., the direction of the $\boldsymbol{B}\text{x}\nabla\boldsymbol{B}$ ion particle drift and the deuterium gas puff rate Γ_{D2} (108 Torr l/s). We found that argon buildup in the main plasma at a *trace* argon injection level was 50%–60% higher in the DN case than in the SN ($dRsep = +1.0$ cm) case under steady state conditions. For these cases, $\Gamma_{Ar} = 0.17$ Torr l/s, $P_{IN} = 6.5$ MW, $\nu_{ELM} \approx 130$ Hz, and $n_e = 0.6 \text{ x } 10^{20}$ m^{-3} (SN) and $0.7 \text{ x } 10^{20}$ m^{-3} (DN). Both SN and DN plasmas were attached at the inner and outer targets in the upper divertor. The DN plasma was attached at the outer target in the lower divertor, as it was in the perturbing argon injection cases discussed below. Analysis of tangential views of the lower divertor in D_α light and CIII line emission indicate that the inner target of the lower (DN) divertor was detached.

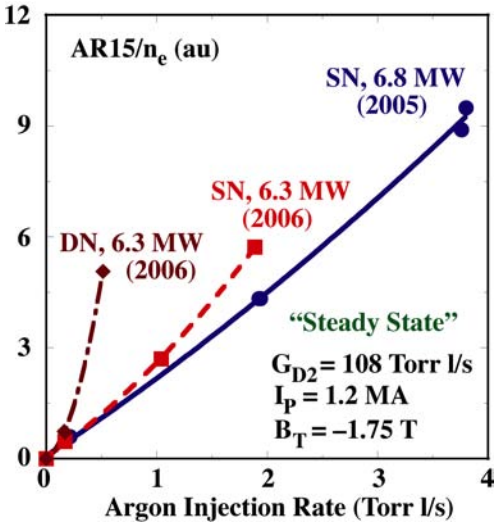

Fig. 6. The main plasma steady state argon concentration is plotted versus the argon injection rate Γ_{Ar} for SN and DN plasma shapes. Included are also SN from the 2005 puff-and-pump campaign.

The difference in argon concentration between DN and SN at *trace* Γ_{Ar} became more pronounced at perturbing Γ_{Ar}. In Fig. 6, core n_{Ar} ($\propto$ ArXV/n_e) is plotted against Γ_{Ar}. For reference, the SN cases from 2005 campaign have been added to the DN and SN cases from 2006. At $\Gamma_{Ar} \approx 0.5$ Torr l/s, n_{Ar} was 4–5 times higher in the DN case than for the SN cases of either 2005 or 2006. Alternatively, 3–4 times the argon injection rate for SNs would be needed to reach a similar argon concentration that was found in the DN case. While under steady puff-and-pump conditions, the DN discharge in Fig. 6 was found to be near its limit Γ_{Ar}. Yet, SN plasmas could tolerate considerably higher values of Γ_{Ar} and remain in ELMing H-mode.

The addition of argon to the DN plasma significantly increased radiated power, but this increase was unequal between divertors (Fig. 7).

Figure 7(a) shows the emissivity distribution just prior to the start of argon injection, and Fig. 7(b) is the emissivity after 2 s of argon injection. Argon injection into the upper PFR resulted in a more pronounced increase in the radiated power from the upper divertor ($P_{R,UP-DIV}$) than from the lower divertor ($P_{R,LOW-DIV}$). Even though the emissivity distributions between the upper and lower divertors were somewhat different prior to the start of argon injection, their integrated radiated powers were comparable, i.e., $P_{R,UP-DIV} \approx P_{R,LOW-DIV} \approx 0.70$ MW. With argon, however, $P_{R,UP-DIV}$ increased almost 50%, while $P_{R,LOW-DIV}$ increased by only $\approx 8\%$. Total radiated power and the radiated power from the main plasma increased by almost 33% and 28%, respectively.

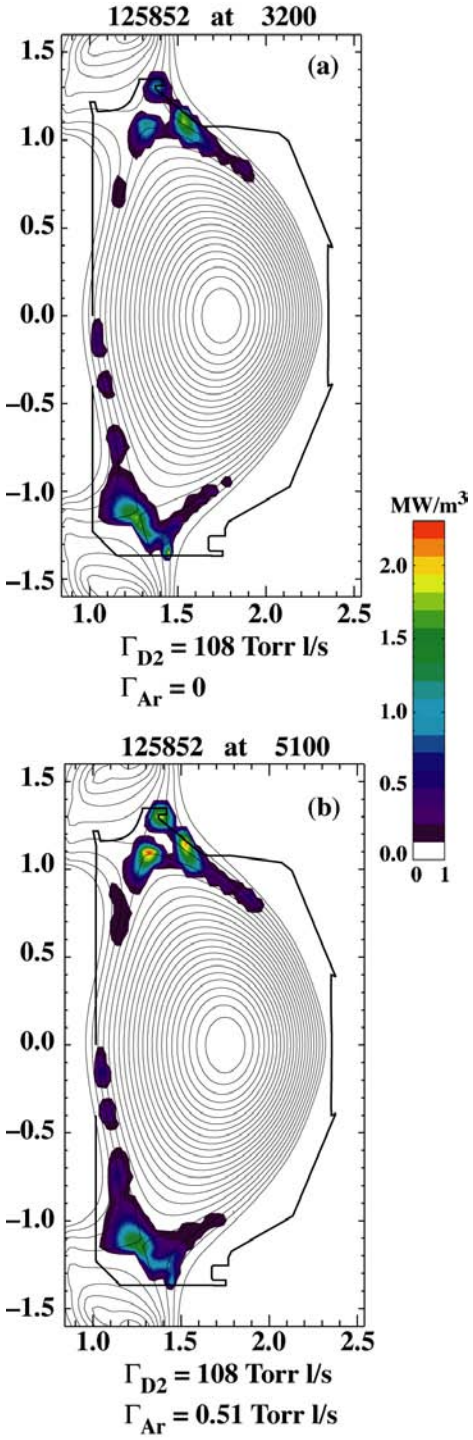

Fig. 7. Argon injection into the private flux region of the upper divertor increased the radiative emissivity much more in the upper divertor than in the lower divertor: (a) pre-argon injection and (b) after 2 s of argon injection.

4. Discussion

Good confinement and low core radiated power for the hybrid SNs were maintained during puff-and-pump, as shown in Section 3(a). Argon puffing directly into the upper outer divertor private flux region, in combination with D_2 injection into the upstream SOL and particle pumping at both divertor targets, reduced $q_{P,OUT}$ by about a factor of 2.5 between Case 1 and Case 3. The reduction in $q_{P,IN}$ was $\leq 20\%$. This difference in heat flux reduction resulted from a greater increase in local emissivity near the outer divertor target than near the inner, caused by a greater concentration of argon near the outer target.

Several factors may have contributed to the asymmetric argon distribution in the SN cases. Proximity of the argon source, located in the PFR near the outer divertor target, to a major *sink* for the argon, the entrance to the outer baffle pumping plenum, may have resulted in a low argon concentration in the outer SOL. For the Ar *neutral*, direct flight across the PFR from the outer divertor target to the inner was blocked by the presence of the dome. The *ionized* Ar in the PFR near the separatrices would be preferentially dragged toward the outer divertor target, because the $E_R \times B$-induced deuteron flow across the PFR is directed from inner target to the outer. Leakage of Ar out of the closed outer divertor was impeded by the enhanced D^+ flow in the SOL directed into that divertor. Finally, Ar that *does* arrive at the inner target can be exhausted by the dome cryopump. Together, these factors would inhibit a buildup of Ar (and Ar-enhanced radiated power) at the inner target, and explain why a large reduction in $q_{P,IN}$ was not observed.

The accumulation of Ar in the main plasma was almost linear with Γ_{Ar}. One expects n_{Ar} to be roughly proportional to $\Gamma_{Ar} - \Gamma_L(\nu_{ELM})$, where $\Gamma_L(\nu_{ELM})$ is the time-averaged Ar losses from the main plasma during ELMs. If $\Gamma_L(\nu_{ELM})$ were constant as Γ_{Ar} was raised, n_{Ar} would be linear with Γ_{Ar}. However, as more Ar concentration increased in the main plasma at higher Γ_{Ar}, $P_{RAD,MAIN}$ increased and ν_{ELM} decreased, so that $\Gamma_L(\nu_{ELM})$ would decrease. The observed reduction in Type-1 ELMing would lead to less effective screening of Ar from the main plasma and a slightly greater than linear response in n_{Ar} to Γ_{Ar}. We also found that the presence of a benign 3/2 NTM did not prevent the n_{Ar}-profile from becoming more peaked than the n_e-profile. Even so, $\varepsilon_{RAD}(\rho)$ was not peaked on axis.

The balanced DN plasmas were found to be much more sensitive to the argon injection rate than corresponding SN plasmas. Previously, deuterium fueling in DN plasmas was shown to be more efficient than in SN plasmas [12]; hence, the injected argon might also display a similar efficient "fueling". The SOL plasmas of DNs differ in two major ways from that of SNs: (1) the characteristic electron temperature for the inboard SOL plasma of the DN is lower than that of the SN, while the SOL density profile is narrower for the DN [13]. Thus, neutral argon on the high field side can penetrate the SOL of the DN more readily than it can for the SOL of the SN. (2) The SOL of the DN is largely quiescent on the inboard side, since ELMs, produced almost exclusively on the low-field side, are cut-off from the high field SOL plasma [14]. This would make it somewhat easier for argon on the high field side of the DN plasma to diffuse to the separatrix into the main plasma during puff-and-pump operation. Furthermore, the inner leg of the lower divertor is observed to be detached in the DN. Consequently, argon that is recycling near the lower outer divertor target would have a nearly direct access to the high field side of the main plasma.

Applying the puff-and-pump approach to hybrid plasmas produced tradeoffs in heat flux reduction, plasma cleanliness, and energy confinement. For the SN hybrid plasmas, the tradeoffs were favorable, e.g., a sharply reduced $q_{P,OUT}$ while maintaining good energy confinement and low fuel dilution. Recent experiments in DNs offer more challenges, since the injected argon penetrates the main plasma more readily than in SNs.

This work was supported by the U.S. Department of Energy under DE-FC02-04ER54698, W-7405-ENG-48, DE-AC05-00OR22725, and DE-AC04-94AL85000.

References

[1] WADE, M.R., et al., Nucl. Fusion **38** (1998) 1839.
[2] GOETZ, J.A., et al., J. Nucl. Mater. **266-269** (1999) 359.
[3] WADE, M.R., et al., Nucl. Fusion **45** (2005) 407.
[4] YUSHMANOV, P.N., et al., Nucl. Fusion **30** (1990) 1999.
[5] PETRIE, T.W., et al., J. Nucl. Mater. **337-339** (2005) 216.
[6] GREENWALD, M., et al., Nucl. Fusion **28** (1988) 2199.
[7] GOHIL, P., et al., Phys. Rev. Lett. **61** (1988) 1603.
[8] WHYTE, D.G., et al., Phys. Plasmas **5** (1998) 3694.
[9] KLEPPER, C.C., HILLIS, D.L., WADE, M.R., et al., Rev. Sci. Instrum. **68** (1997) 400.
[10] HULSE, R.A., Nucl. Technol. Fusion **3** (1983) 259.
[11] SUMMERS, H.P., "Atomic data and analysis structure," JET Joint Undertaking Report JET-IR(94)06 (1994).
[12] PETRIE, T.W., et al., J. Nucl. Mater. **266-269** (1999) 642.
[13] PETRIE, T.W., et al., J. Nucl. Mater. **313-316** (2003) 834.
[14] PETRIE, T.W., et al., Nucl. Fusion **43** (2003) 910.